Geophysical Research Letters

RESEARCH LETTER
10.1029/2023GL103334

A New Multi-Method Assessment of Stratospheric Sulfur Load From the Okmok II Caldera-Forming Eruption of 43 BCE

Ally Peccia[1,2], Yves Moussallam[1,2], Terry Plank[1,2], Kevin DallaSanta[3,4], Lorenzo Polvani[1,2,3], Alain Burgisser[5], Jessica Larsen[6], and Janet Schaefer[7]

[1]Lamont-Doherty Earth Observatory, Columbia University, Palisades, NY, USA, [2]Department of Earth and Environmental Sciences, Columbia University, Palisades, NY, USA, [3]Department of Applied Physics and Applied Mathematics, Columbia University, New York, NY, USA, [4]NASA Goddard Institute for Space Studies, New York, NY, USA, [5]University Grenoble Alpes, University Savoie Mont Blanc, CNRS, IRD, IFSTTAR, ISTerre, Grenoble, France, [6]Department of Geosciences, Geophysical Institute, Alaska Volcano Observatory, University of Alaska, Fairbanks, Fairbanks, AK, USA, [7]State of Alaska Division of Geological and Geophysical Surveys, Alaska Volcano Observatory, Fairbanks, AK, USA

Abstract The 43 BCE eruption of Okmok Volcano has been proposed to have had a significant climate cooling impact in the Northern Hemisphere. In this study, we quantify the climate cooling potential of the Okmok II eruption by measuring sulfur concentration in melt inclusions (up to 1,606 ppm) and matrix glasses and estimate a total of 62 ± 16 Tg S released. The proportion reaching the stratosphere (2.5%–25%, i.e., 1.5–15.5 Tg S) was constrained by physical modeling of the caldera-collapse eruption. Using the NASA Goddard Institute for Space Studies E2.2 climate model we found a linear response between cooling and stratospheric sulfur load (0.05–0.08°C/Tg S). Thus, the 1–2°C of cooling derived from proxy records would require 16–32 Tg sulfur injection. This study underscores the importance of combining approaches to estimate stratospheric S load. For Okmok II, we find all methods are consistent with a range of 15–16 Tg S.

Plain Language Summary Gaseous sulfur released in explosive volcanic eruptions can reflect incoming solar radiation in the stratosphere and cool the Earth's surface. Here, we calculate the total amount of sulfur released in the 43 BCE caldera-forming eruption of Okmok Volcano, Alaska by measuring the concentration of sulfur dissolved in magma prior to the eruption. We find that the total sulfur load from the Okmok II eruption is one of the largest in the last 2,500 years, and we use climate models to simulate cooling and precipitation anomalies associated with total or partial injection of volcanic sulfur into the stratosphere. However, the estimated sulfur load is larger than that predicted by sulfur signals preserved in ice cores, and physical modeling of the eruption suggests that only a proportion of the sulfur released reached stratospheric altitudes. Further, comparison of temperature reconstructions from tree ring and cave deposit proxies with climate model results show the cooling associated with the eruption requires only a fraction of the total sulfur load. Thus, we propose that only a quarter of the total sulfur released in the eruption made it to the stratosphere, responsible for 1–2°C of cooling in the year following the eruption.

Key Points:

- Petrologic evidence suggests a total of 62 Tg S was released in the caldera-forming eruption of Okmok Volcano in 43 BCE
- Climate models respond linearly to stratospheric sulfur loads. 1–2°C cooling from proxy records suggests 16–32 Tg S injection
- A physical model constrains the proportion of stratospheric sulfur to 2.5%–25%; thus we find a common range for all methods of 15–16 Tg S

Supporting Information:

Supporting Information may be found in the online version of this article.

Correspondence to:

A. Peccia,
asp2201@columbia.edu

Citation:

Peccia, A., Moussallam, Y., Plank, T., DallaSanta, K., Polvani, L., Burgisser, A., et al. (2023). A new multi-method assessment of stratospheric sulfur load from the Okmok II caldera-forming eruption of 43 BCE. *Geophysical Research Letters*, *50*, e2023GL103334. https://doi.org/10.1029/2023GL103334

Received 22 FEB 2023
Accepted 13 SEP 2023

Author Contributions:

Conceptualization: Ally Peccia, Yves Moussallam, Terry Plank, Kevin DallaSanta, Lorenzo Polvani, Alain Burgisser
Data curation: Ally Peccia, Kevin DallaSanta
Formal analysis: Ally Peccia, Kevin DallaSanta
Funding acquisition: Yves Moussallam, Terry Plank, Lorenzo Polvani
Investigation: Ally Peccia, Yves Moussallam, Terry Plank, Kevin DallaSanta, Lorenzo Polvani

1. Introduction

What will be the climate impact of the next major volcanic eruption? The answer to this question lies in our understanding of past notable events. Here we explore the volcanic drivers and climatic response of the Okmok II eruption, Alaska. This eruption was recently recognized by McConnell et al. (2020) as the source of Greenland ice core sulfate peaks at 43 BCE, and implicated as the cause for regional temperature and precipitation anomalies that may have led to social unrest in the late Roman Republic and Ptolemaic Kingdom.

Okmok II consisted of two eruptive phases, the first producing ~0.85 km^3 bulk (0.6 km^3 DRE) of Plinian rhyodacite and subsequent andesite fall deposits across Umnak Island, and the second major caldera-forming phase producing ~50 km^3 bulk (29 km^3 DRE) of pyroclastic density current (PDC) deposits (Burgisser, 2005; Larsen et al., 2007; Wolfe, 2001). The composition of the tephra recovered from the GISP2 ice core aligns best with the material erupted as basaltic andesite PDCs (McConnell et al., 2020 and see below). This suggests that the PDC material was lofted high enough to be dispersed to the opposite side of the Northern Hemisphere, prompting further study of pyroclastic-associated plumes and caldera collapse via physical modeling (Burgisser et al., 2023).

Methodology: Ally Peccia, Yves Moussallam, Terry Plank, Kevin DallaSanta, Lorenzo Polvani, Alain Burgisser
Resources: Yves Moussallam, Terry Plank, Lorenzo Polvani, Jessica Larsen, Janet Schaefer
Supervision: Yves Moussallam, Terry Plank, Lorenzo Polvani, Alain Burgisser
Validation: Ally Peccia, Yves Moussallam, Terry Plank, Kevin DallaSanta, Lorenzo Polvani, Alain Burgisser
Visualization: Ally Peccia, Terry Plank, Kevin DallaSanta, Alain Burgisser
Writing – original draft: Ally Peccia, Kevin DallaSanta
Writing – review & editing: Ally Peccia, Yves Moussallam, Terry Plank, Kevin DallaSanta, Lorenzo Polvani, Alain Burgisser, Jessica Larsen

The primary goal of this study is to provide the first petrological measurements of the total amount of sulfur released by Okmok II magma. The other goal is to estimate the fraction of this load injected to the stratosphere, critical to determining its climate impact. This quantity is challenging to determine by any one method, and the novelty of our study is that we employ three independent methods and data sets for estimating stratospheric sulfur: (a) ice sheet deposition and sulfur isotopes, (b) global climate model and climate proxy data, and (c) total petrologic sulfur load and eruption dynamics modeling for stratospheric injection.

2. Materials and Methods

Okmok II PDC and andesite fall samples were selected for melt inclusion study (Figure 1a, Table S3 in Supporting Information S1). Polished crystals and matrix glasses from four samples were measured by electron microprobe for major element composition and sulfur concentration. Selected melt inclusions and matrix glasses were then measured for water and sulfur content by ion microprobe (Figure 1d; Texts S3 and S4 in Supporting Information S1).

To quantify the climate impacts of different stratospheric sulfur injection amplitudes, we simulated the effect of the Okmok II eruption on the global climate system using the NASA Goddard Institute for Space Studies (GISS) Model E2.2 (Orbe et al., 2020; Rind et al., 2020). It was configured following DallaSanta and Polvani (2022) and is a state of the art atmosphere-ocean-land-sea ice coupled model which participated in the Coupled Model Intercomparison Project, Phase 6 (CMIP6) (Text S7 in Supporting Information S1).

3. Total Sulfur Load

3.1. Melt Inclusion Composition

The sulfur concentrations in 19 melt inclusions from Okmok II range from 152 to 1,606 ppm S (with 10% relative uncertainty in the ionprobe analysis) in melt compositions that span from basaltic to rhyodacitic (51–65 wt% SiO_2, concentrations expressed volatile-free). To estimate sulfur load, it is critical to determine the melt inclusion compositions that best reflects the ~50 km^3 of bulk PDC magma, as both the whole rocks and matrix glasses are degassed in sulfur. The more evolved composition of the GISP2 tephra (54.7–59.9 wt% SiO_2) and PDC matrix glass (57.1–60.8 wt% SiO_2) is inferred to be the result of degassing-driven crystallization of microlites upon ascent as described by Larsen et al. (2007), and thus does not represent the bulk PDC composition (Figure 1b; Text S5 in Supporting Information S1). The MI compositions in AOK147-plag have SiO_2 (55.2–56.4 wt%) that overlap best with the PDC whole rocks (54.6–55.7 wt% SiO_2), which we take to best represent the bulk composition of the PDC magma (Figure 1b). These inclusions have the highest sulfur concentrations and are in equilibrium with their plagioclase hosts and the bulk PDC composition, suggesting they represent the original volatile content of the magma before degassing, with sulfide saturation inferred from the Cu-Th trend in Okmok whole rocks (1,263–1,606 ppm S, Figure 1c, Text S6 in Supporting Information S1). Selection of these inclusions is critical in accounting for the sulfur concentration in the parental PDC magma body at depth, which would otherwise be underestimated by ~1,000 ppm S if the petrologic method was applied to melt inclusions similar in composition to the matrix glass (Su et al., 2016; Figure 1c). We thus take the pre-eruptive concentration for the Okmok II PDC magma as the maximum sulfur measured in these inclusions: 1,606 ± 160 ppm. Total sulfur concentration in the parental PDC magma could be even higher due to minor sulfide fractionation (see Cu-Th systematics in Figure S4 in Supporting Information S1) or prior degassing.

3.2. Total Mass Erupted and Total Sulfur Load

Calculating the total sulfur load from Okmok II requires an estimate of the erupted mass. PDCs account for 98% of the volume erupted in Okmok II, and thus represent the most important volume component for estimating total sulfur load. Burgisser (2005) estimated a total of 24 km^3 of PDC deposits on Umnak and Unalaska Island, but recognized a large uncertainty in the volume of underwater deposits. To address this, we assume two areas of deposition around Umnak Island that extend the thickness of the deposits measured on land to sea (see Figure S3 in Supporting Information S1). This produces an additional 25 km^3 of pyroclastic flows deposited underwater for a total volume during Okmok II PDC stage of 50 ± 10 km^3, consistent with the volume of the caldera (Burgisser, 2005). We calculate a total erupted magma mass of $4.29 \pm 1.01 \times 10^{13}$ kg, based on average deposit density and corrections for pre-existing lithic material and deposit void fraction (Burgisser, 2005; Text S1 in Supporting Information S1). The sulfur load is then derived from Equation 1 of Devine et al. (1984):

$$M_s = M_v(1 - W_x)(C_i - C_m) \quad (1)$$

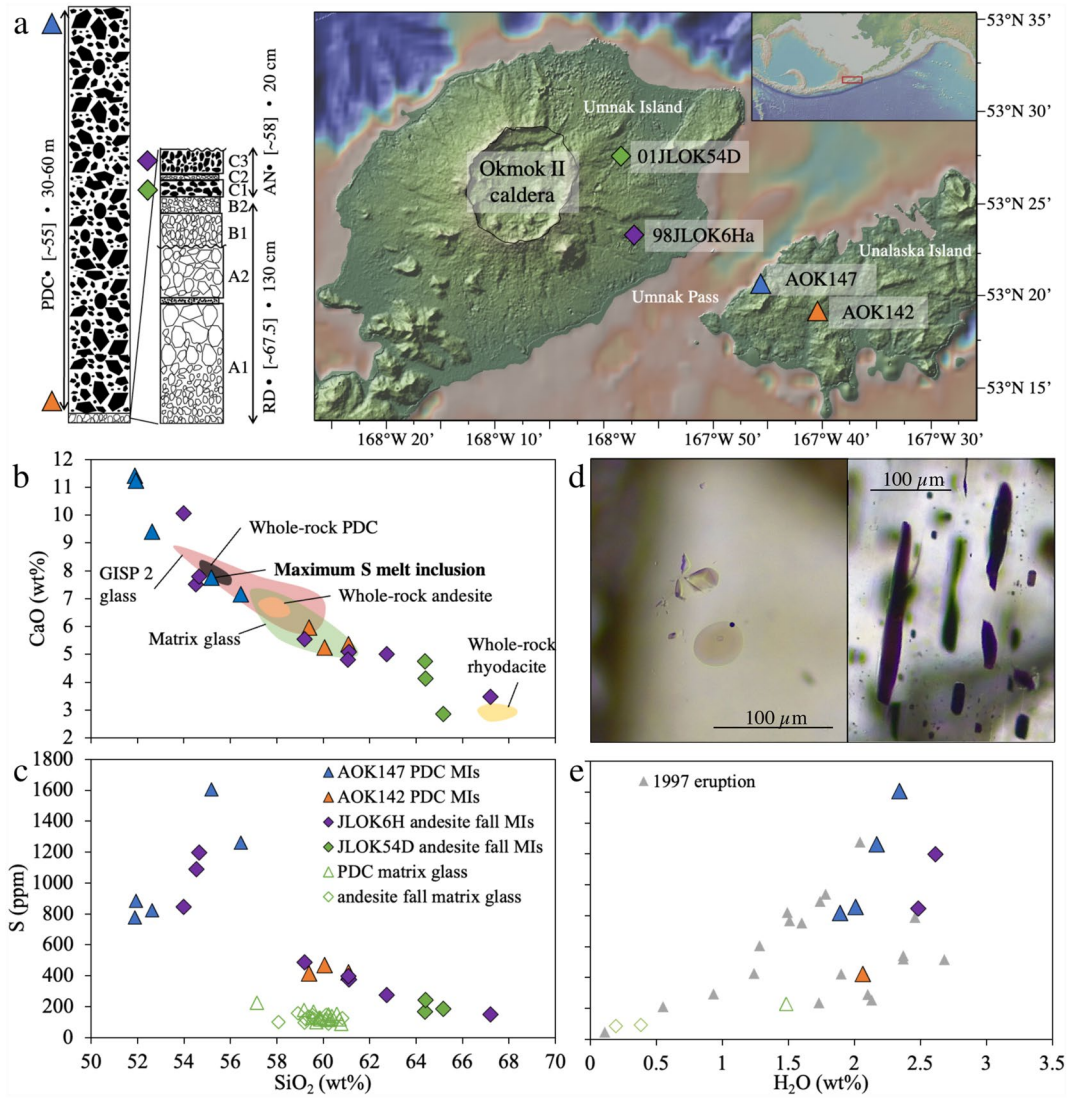

Figure 1. Stratigraphic sequence of Okmok II units (a, left) and map of sample locations across Umnak and Unalaska Islands ((a), right). Units are labeled by type and composition (RD = rhyodacite fall, AN = andesite fall, and PDC = pyroclastic density current), with bulk rock SiO_2 wt% in brackets. Fall deposits are noted by units (A, B, C) identified in Burgisser (2005), and are scaled relative to maximum deposit thickness. Pyroclastic flow facies have an average thickness of 30–60 m depending on distance from the caldera. Panels (b, c) show sulfur and major element concentrations in melt inclusions, matrix glasses, and whole-rocks from Okmok II. CaO and SiO_2 are reported volatile-free, normalized to 100%. Matrix glasses are plotted together in panel (b), and separated in panel (c). They largely overlap in our data set. Photomicrographs (d) are of representative olivine-hosted melt inclusions from the JLOK6H andesite fall (left) and plagioclase-hosted melt inclusions from pyroclastic density current deposit sample AOK147 (which contains the maximum S concentrations). The H_2O and S concentrations in panel (e) were measured by ionprobe, and include melt inclusion measurements from the 1997 eruption of Okmok from Zimmer et al. (2010). Panel (a) made with GeoMapApp (Ryan et al., 2009).

where M_s is the mass of sulfur erupted, W_x is the mass fraction of crystals, C_i is the concentration of sulfur as measured in melt inclusions, and C_m is the concentration of sulfur as measured in degassed matrix glass. W_x is taken as 1.7% ± 1.8% (Burgisser, 2005). C_i is 1,606 ± 160 ppm (as above) and C_m is 127 ± 23 ppm S. Thus, ~1,500 ppm of sulfur was degassed during this eruption, producing a total sulfur load of 62 ± 16 Tg S (Equation 1, Table S1 in Supporting Information S1). This is likely a minimum estimate for total Okmok II sulfur emission, given our assumptions of zero pre-exsolved gas phase. Further, seawater vapourization as a result of contact with hot PDC material could have led to additional S release (Rowell et al., 2022), though it's unlikely that this source would reach a significant altitude (Dufek et al., 2007).

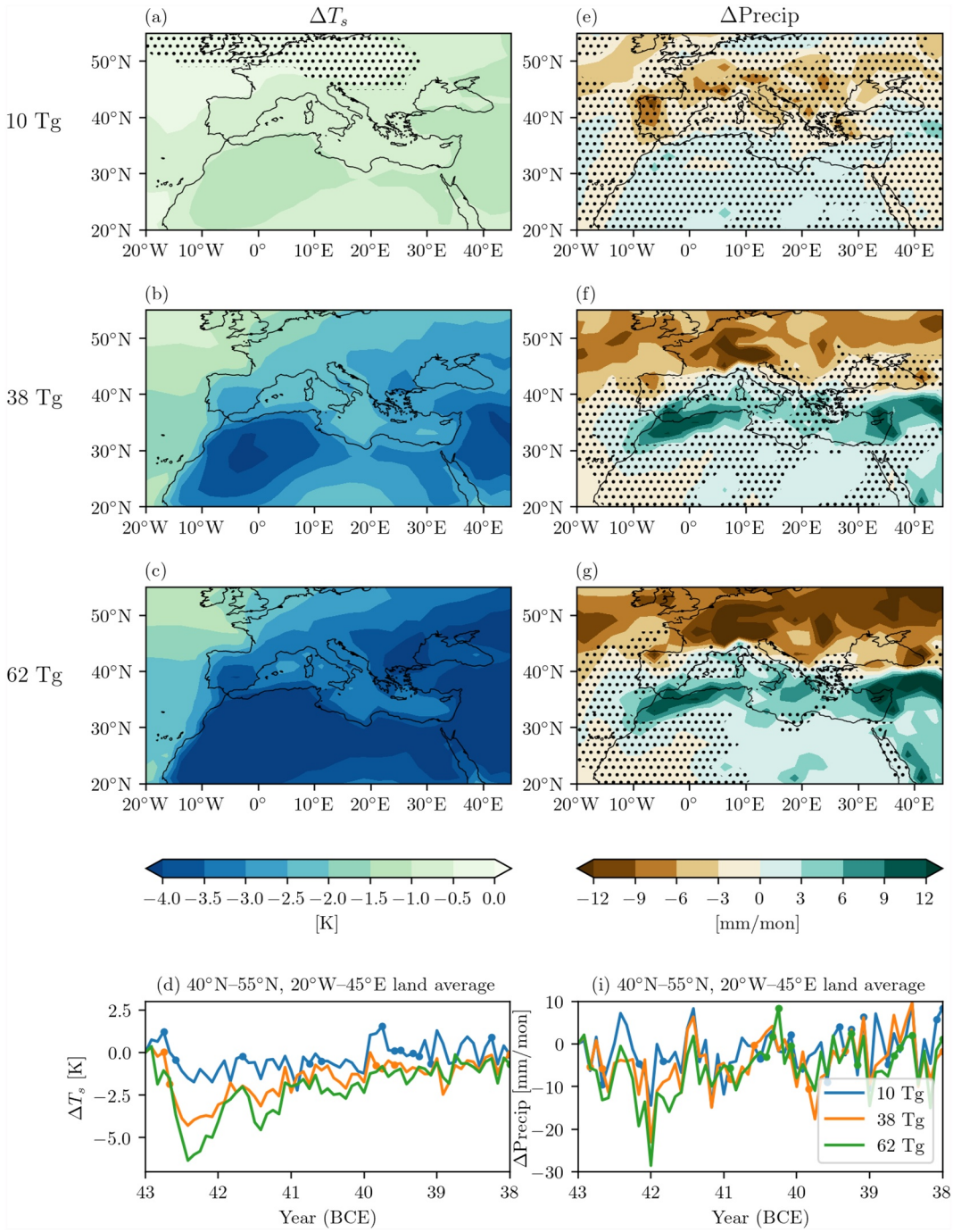

Figure 2. Impact of Okmok II eruption on Mediterranean surface temperature (column 1) and precipitation (column 2). The responses are defined as ensemble-averaged departures from the corresponding control run, averaged over 43 and 42 BCE. Stippling indicates an inability to reject the null hypothesis at 95% confidence. The three sulfate amplitudes are labeled for rows 1–3. Row 4 shows the time evolution of the responses, averaged over the specified region. Dots indicate where all 10 members are less than zero.

3.3. Climate Model Scenarios

We performed model simulations to study the effect of three different stratospheric S loads: 62 Tg (total petrologic S load), 38 Tg (estimated by McConnell et al., 2020 from ice core load), and 10 Tg (lower bound) and averaged response over 43 and 42 BCE, when the signal is largest (Figure 2d). In the Mediterranean region, the

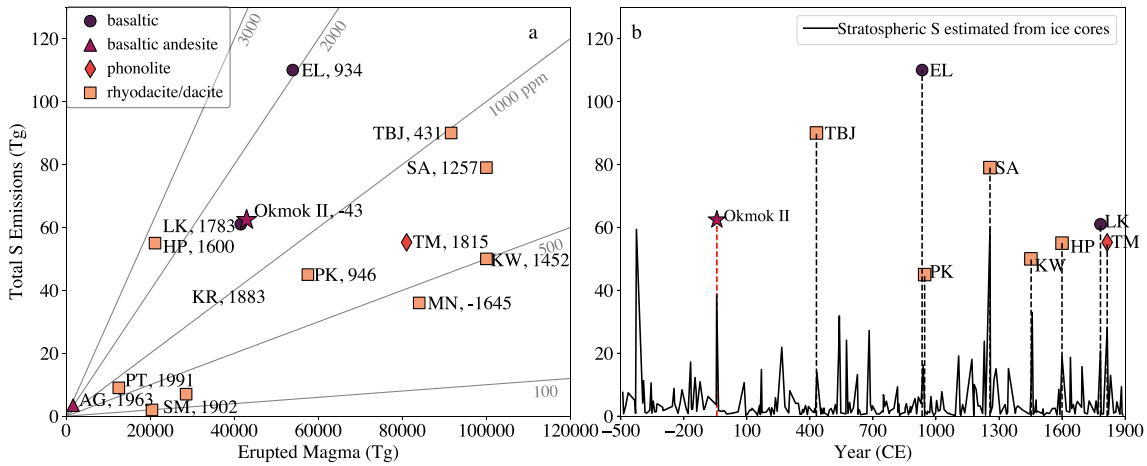

Figure 3. Okmok II sulfur load compared with (a) sulfur emission estimates of other historical eruptions (Table S2 in Supporting Information S1) and (b) ice core-based estimates of stratospheric sulfur loading (b). Lines in (a) show sulfur emissions for magmas that undergo 100, 500, 1,000, 2,000, and 3,000 ppm of sulfur degassing, for reference. Dashed lines in panel (b) show the offset between total sulfur emission from petrological studies and the stratospheric S estimated from ice core studies. The difference between the two likely reflects variable stratospheric injection of the total sulfur load during any given eruption. Eruptions are colored by dominant composition, with eruption years noted. Dates in panel (b) extend from 500 BCE to 1990 CE, reflecting the coverage of the ice core record presented in the eVolv2k v3 database (Toohey & Sigl, 2017). Eruption name codes: (AG: Agung, EL:E ldgja, HP: Huayanaputina, LK: Laki, KR: Krakatau, KW: Kuwae, MN: Minoan/Thera, PK: Paektu, PT: Pinatubo, SA: Samalas, SM: Santa Maria, TBJ: Ilopango TBJ, and TM: Tambora).

magnitude of cooling ranges from 1 to 4K (Figures 2a–2c). Land surface cooling observed with 38 Tg S agree closely with McConnell et al. (2020), who used a different climate model than ours, but an identical aerosol forcing model. Over the Northern Hemisphere (Figures S1a–S1d in Supporting Information S1), we observe highly significant surface temperature responses. The milder responses over Northern Eurasia, as compared to North America, are associated with a positive phase of the Northern Annular Mode in boreal winter, which emerges for sufficiently large eruptions (DallaSanta & Polvani, 2022). The lack of response in the Southern Hemisphere is due to the Easy Volcanic Aerosol (EVA) parameterization of hemispheric asymmetry, though a small volcanic sulfate peak is observed in Antarctic ice cores around the same time (Figure S1 in Supporting Information S1; Toohey et al., 2016). Notably, the climate response, as defined by the ensemble averaged departure from control run, shows roughly linear cooling as a function of S load (0.05–0.08°C cooling/Tg S) (Figure 4).

Overall, we find reduced precipitation over Northern Europe and increased precipitation over Southern Europe following the eruption, with magnitudes up to 12 mm/month. Our dipole response for 38 Tg is slightly shifted in latitude from that in McConnell et al. (2020), pointing to intermodel uncertainties. As with temperature, the precipitation response strengthens approximately linearly with stratospheric sulfur injection mass, with significance emerging at 38 Tg S (Figure 2f) and strengthening at 62 Tg S (Figure 2g). However, the month-to-month spread across ensemble members is high (Figure 2h). Thus, the Roman Empire likely experienced overall precipitation changes after the eruption, but any given month could have been wetter or drier. The precipitation changes over Africa reflect heightened interannual variability due to contraction of the Hadley Cell, which could have led to drying at the Nile headwaters (Figures 2e–2i, Figures S1e–S1i in Supporting Information S1), consistent with historical records (McConnell et al., 2020). On a global scale (Figures S1e–S1i in Supporting Information S1), the precipitation response is more robust, associated with changes to the zonally symmetric circulation.

Lastly, we find that the month of eruption does not appear to be critical for the temperature and precipitation impacts (Figure S2 in Supporting Information S1). This provides confidence that our results are meaningful for historical interpretation, as the actual eruption month of the Okmok II eruption is not known.

4. Multi-Method Assessment of Stratospheric S Injection

4.1. Among the Largest Sulfur Loads in History

A petrologic sulfur load of 62 Tg S for Okmok II is on par with historical eruptions of similar size (Laki, Samalas, Paektu, Minoan), and ranks as one the largest volcanic sulfur loads in the last 2,500 years (Figure 3). Comparable eruptions have been linked to climate instability and major historical milestones: the 1783 flood-lava eruption

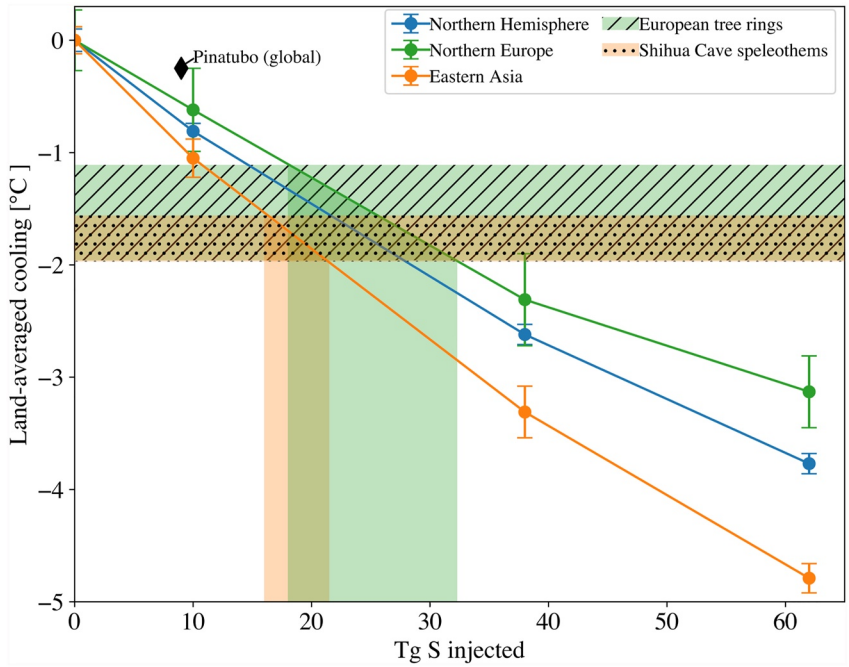

Figure 4. Land-averaged cooling response following modeled stratospheric sulfur injections (10, 38, 62 Tg S) from Okmok II over three representative areas: Northern Europe (green line, 40°–70°N, 10°W, 30°E), Asia (orange line, 30°–55°N, 40°, 140°E), and the Northern Hemisphere (blue line). The three injection scenarios show a roughly linear cooling response for all regions. Proxy cooling reconstruction is denoted by the shaded areas: tree ring temperature reconstructions from Northern Europe predict −1.52 ± 0.42°C of cooling in 43 BCE (Luterbacher et al., 2016), while a Chinese speleothem record predicts −1.76 ± 0.2°C of cooling within a 5-year dating uncertainty (Tan et al., 2003). Combined with climate model runs, overlapping proxy evidence suggests a stratospheric sulfur load of 18–22 Tg S. Stratospheric sulfur injection and observed change in global mean surface temperature from the 1991 eruption of Pinatubo is noted for reference (Guo et al., 2004; Pauling et al., 2023).

of Laki emitted around 60 Tg of sulfur and drove significant cooling in the Northern Hemisphere (Schmidt et al., 2011; Thordarson & Self, 2003; Zambri et al., 2019), while the 1257 eruption of Mt. Samalas generated ∼1–2°C global cooling and has been connected with the initiation of the Black Death in Europe (Büntgen et al., 2022; Fell et al., 2020; Guillet et al., 2017). Notably, petrologic evidence suggests very little halogen degassing from Okmok II (∼0 Tg for Cl and F), with matrix glass concentrations of Cl and F near or greater than that observed in melt inclusions.

Only S injected into the stratosphere exerts a climate cooling influence (e.g., Robock, 2000). Sulfate concentrations in ice cores have been used to estimate stratospheric sulfur loading, relying on the transport and deposition of volcanic sulfate aerosols to ice sheets 1–2 years post-eruption (Toohey & Sigl, 2017). While this strategy is useful for identifying the timing of large eruptions and their relative magnitudes, it does not provide source constraints nor does it distinguish stratospheric fall-out versus sulfur transported through the troposphere (Marshall et al., 2021). In Figure 3b, we compare petrological estimates of sulfur load and ice core estimates over the past 2,500 years, and find that petrologic estimates are systematically higher than the modeled ice core deposition. This offset likely reflects variable stratospheric injection due to the physical dynamics of any given eruption and illustrates the importance of studies of past volcanic sulfur loads.

To address partial stratospheric injection of the total S load from the Okmok II eruption, we compare below three independent methods: (a) ice core deposition, (b) eruption dynamics, and (c) climate proxy data.

4.2. Stratospheric Injection From Ice Cores

Synchronized estimates made by Toohey and Sigl (2017) predict stratospheric sulfur injection of 38.6 ± 11.3 Tg S from Okmok II based on its source location and ice core sulfate concentrations. McConnell et al. (2020) assumed all of this was stratospheric, and used this as input to their climate model. A recent study (Pearson et al., 2022)

proposes an even larger stratospheric sulfur load of 48 ± 15 Tg S, which would represent ~77% of the total erupted sulfur given our petrologic estimate. This same study, however, makes the important point that some ice-deposited S will be tropospheric, especially for volcanoes like Okmok which are relatively proximal to Greenland.

A closer examination of mass independent fractionation in sulfur isotopes (S-MIF) may be used to resolve the stratospheric versus tropospheric ice deposition of sulfur (Burke et al., 2019). A study of the Aniakchak II eruption (1628 BCE) uses mass balance, along with triple isotope measurements of sulfate deposited in Greenland to estimate the proportion of ice-deposited sulfate that reached the stratosphere (Pearson et al., 2022). The Aniakchak II eruption, which had a similar ice deposition (52 Tg) to Okmok II (48 Tg) and is at similar latitude in Alaska (56.9°N) to Okmok (53.4°N), deposited a sulfur peak on Greenland that was calculated to be 61% stratospheric and 39% tropospheric. Given that the magnitude of the S-MIF peak measured for Okmok was much smaller than that for Aniakchak ($\Delta^{33}S_{max}$ = 0.20‰ for Okmok II vs. $\Delta^{33}S_{max}$ = 1.30‰ for Aniakchak II), the stratospheric proportion for the total volcanic S deposited following the Okmok II eruption will be <61%. As the measurements in McConnell et al. (2020) did not include key sulfur concentrations or background isotope ratios, it is not currently possible to carry out a meaningful sulfur mass balance for Okmok. Furthermore, S-MIF may not occur in the lower stratosphere at high latitudes, and thus relying solely on $\Delta^{33}S$ may result in an underestimation of stratospheric sulfur injection and resulting climate cooling (Thordarson & Self, 2003). Nonetheless, the existing measurements suggest a smaller stratospheric proportion for Okmok II versus Aniakchak II, and thus we can conclude that <29 Tg (61% of 48 Tg) of Okmok II sulfur load measured in ice cores was stratospheric. This would constitute <47% of the total S erupted.

4.3. Stratospheric Injection From Eruption Dynamics Models

The presence of basaltic andesite tephra and S-MIF in Greenland ice cores indicate that the Okmok II PDC material reached across the Northern Hemisphere and had a stratospheric component (McConnell et al., 2020). This presents a conundrum, as the Okmok II PDC deposits are not associated with an airfall deposit. In order to address how a predominantly pyroclastic flow-generating eruption could also produce stratospheric sulfur and hemispheric ash without producing a Plinian air-fall, a companion study uses a numerical model to explore the conditions that could lead to this eruptive behavior.

Burgisser et al. (2023) apply the MFIX-TFM two-phase flow model to simulate the dynamics of PDC emplacement. Model results are constrained by field stratigraphic observations of asymmetric deposition, maximum flow runout, a lack of airfall deposits and total mass erupted, with the stratospheric injection of gas during the eruption estimated via mass balance based on the fraction of stratospheric solids.

The results of this physical model indicate that 2.5%–25% of the solids and gases from the PDC phase of the Okmok II eruption would be injected into the stratosphere (Burgisser et al., 2023). The low proportion of stratospheric injection reflects the lack of an airfall deposit from the central plume, with the majority of stratospheric injection occurring via successive pulses of co-ignimbrite material issued from the main pyroclastic flows. We note that complex eruption dynamics may also affect the transport of S into the stratosphere, such as scavenging in a water-rich plume (Thordarson et al., 1996). Nevertheless, if only 2.5%–25% of the total Okmok II sulfur is stratospheric, that would result in a stratospheric injection of 1.55–15.5 Tg, well below the 29 Tg maximum outlined above based on ice deposition.

4.4. Constraints From Climate Models and Proxies

Temperature proxy evidence from tree ring and speleothem records (McConnell et al., 2020; Sigl et al., 2015) indicate >2°C cooling in the Northern Hemisphere around the time of the Okmok II eruption. As discussed above, our climate modeling indicates a roughly linear relationship between cooling and mass of S injected into the stratosphere (Figure 4). Thus, the amount of cooling recorded by temperature proxies can constrain the amount of stratospheric S needed to create such a signal.

Temperature-sensitive trees in Scandinavia and Austria indicate 1.52 ± 0.42 (1σ) °C of cooling in 43 BCE (Luterbacher et al., 2016). The Shihua Cave temperature reconstruction suggests −1.76 ± 0.20 (1σ) °C (Tan et al., 2003). Taken together, these proxies indicate a conservative 1.1–2.0°C of cooling. Comparing the cooling recorded by European trees (1.1–1.9°C) to the land-averaged cooling response over Northern Europe

predicted by our model, we infer a stratospheric sulfur injection of 18–32 Tg (Figure 4). The Asia-averaged model applied to the Shihua Cave speleothems suggests 16–22 Tg S injection. The two overlap in the range of 20 ± 2 Tg.

4.5. Multi-Method Convergence of Stratospheric S Injection

The upper limit from the eruption model (15.5 Tg) approaches the lower limit of the climate model (16 Tg, as discussed above) and both are permissible given the upper bound from ice deposition (29 Tg). Thus, 15–16 Tg of stratospheric S from Okmok II is consistent with all data, models and approaches.

Despite this coherence, it is worth considering the uncertainties due to the sparsity of data and number of assumptions. It is possible that additional gaseous sulfur could have been injected during the rhyodacitic Plinian phase that preceded the PDCs and caldera collapse. However, the lack of any glass >60% SiO_2 in the Greenland ice cores is inconsistent with the earlier Plinian phases producing a major stratospheric load. Alternatively, it is possible that our petrologic estimate is too low. In order to overlap with the proxy cooling-based estimate for Okmok II (18–22 Tg S), and assuming a 25% stratospheric portion, the total petrologic load would have to be increased to 80 Tg S. A higher petrologic load could be achieved with additional MI measurements that could extend to S concentrations higher than 1,600 ppm, although we note that Zimmer et al. (2010) measured less than 1,300 ppm in all 20 MI from several more recent mafic eruptions of Okmok (Figure 1e). A less conservative estimate of total eruptive volume, or the addition of exsolved sulfur from an unerupted primitive parent could also supply an additional sulfur load.

Conversely, the observed climate cooling could be overestimated. Proxy estimates for cooling on interannual timescales are relatively sparse due to the lack of ancient tree ring records. It is also questionable how well a regionally averaged ensemble of climate models might relate to location-specific (and seasonally specific) data. The GISS climate model results are also very likely to depend on the injection height and aerosol size, and the EVA model used here may not be a good representation of the Okmok II eruption.

Regardless, all evidence suggests less than half of the total Okmok II petrologic sulfur load was injected into the stratosphere, where it produced a significant climate cooling effect. We see the relative agreement in multiple reconstructions as a success that demonstrates the utility of this three-pronged approach to evaluate other eruptions with more robust climate proxy data.

5. Conclusions

The Okmok II eruption released a total sulfur load of 62 ± 16 Tg S, one of the largest estimated sulfur loads in recorded history. However, eruption dynamics models and ice core S-MIF data suggest that much of the sulfur released during Okmok II did not reach the stratosphere. Thus, only a fraction of this total load was available to impact surface climate. Comparison of model-generated climate anomalies with coincident cooling recorded by tree ring and speleothem proxies suggests that a stratospheric sulfur load of 18–22 Tg is consistent with the observed climate effect. This constitutes ∼30% of the total petrologic sulfur load, in good agreement with the upper end of stratospheric injection predicted by physical modeling (25%) and permissible given the ice core S-MIF (<61%).

Moreover, we find a systematic mismatch between petrological and ice core estimates of volcanic sulfur loads, suggesting that partial stratospheric injection should be considered when examining other large eruptions. Okmok II serves as a case study for an interdisciplinary approach to reconstructing major historical eruptions and their related impacts—one that combines petrological source constraints, physical modeling, and climate models to interpret the ice core record.

Data Availability Statement

The data used for the petrological characterization of Okmok II in this study are available to download via the EarthChem repository: https://doi.org/10.26022/IEDA/112955.

Acknowledgments
We gratefully acknowledge the Alaska Volcano Observatory and Alaska Geologic Materials Center repositories for providing samples. We thank Celine Martin, Yunbin Guan, Henry Towbin, Shuo Ding, and Sarah Shi for assistance in sample preparation and measurement. The ancestral homelands of the Unangan people include Okmok Volcano. We respect and honor the past, present, and future Unangan people and their land. The work of Kevin DallaSanta and Lorenzo Polvani was funded in part by a Grant of the U.S. National Science Foundation to Columbia University. We thank reviewers Bruno Scaillet and Thor Thordarson and editor Christian Huber for their constructive feedback, which helped to improve this paper.

References

Büntgen, U., Smith, S. H., Wagner, S., Krusic, P., Esper, J., Piermattei, A., et al. (2022). Global tree-ring response and inferred climate variation following the mid-thirteenth century Samalas eruption. *Climate Dynamics*, *59*(1), 531–546. https://doi.org/10.1007/s00382-022-06141-3

Burgisser, A. (2005). Physical volcanology of the 2,050 BP caldera-forming eruption of Okmok volcano, Alaska. *Bulletin of Volcanology*, *67*(6), 497–525. https://doi.org/10.1007/s00445-004-0391-5

Burgisser, A., Peccia, A., Plank, T., & Moussallam, Y. (2023). Numerical simulations of the latest caldera-forming eruption of Okmok volcano, Alaska. arXiv.Org. Retrieved from https://arxiv.org/abs/2310.05516v1

Burke, A., Moore, K. A., Sigl, M., Nita, D. C., McConnell, J. R., & Adkins, J. F. (2019). Stratospheric eruptions from tropical and extra-tropical volcanoes constrained using high-resolution sulfur isotopes in ice cores. *Earth and Planetary Science Letters*, *521*, 113–119. https://doi.org/10.1016/j.epsl.2019.06.006

DallaSanta, K., & Polvani, L. M. (2022). Volcanic stratospheric injections up to 160 Tg(S) yield a Eurasian winter warming indistinguishable from internal variability. *Atmospheric Chemistry and Physics*, *22*(13), 8843–8862. https://doi.org/10.5194/acp-22-8843-2022

Devine, J. D., Sigurdsson, H., Davis, A. N., & Self, S. (1984). Estimates of sulfur and chlorine yield to the atmosphere from volcanic eruptions and potential climatic effects. *Journal of Geophysical Research*, *89*(B7), 6309–6325. https://doi.org/10.1029/JB089iB07p06309

Dufek, J., Manga, M., & Staedter, M. (2007). Littoral blasts: Pumice-water heat transfer and the conditions for steam explosions when pyroclastic flows enter the ocean. *Journal of Geophysical Research*, *112*(B11), B11201. https://doi.org/10.1029/2006JB004910

Fell, H. G., Baldini, J. U. L., Dodds, B., & Sharples, G. J. (2020). Volcanism and global plague pandemics: Towards an interdisciplinary synthesis. *Journal of Historical Geography*, *70*, 36–46. https://doi.org/10.1016/j.jhg.2020.10.001

Guillet, S., Corona, C., Stoffel, M., Khodri, M., Lavigne, F., Ortega, P., et al. (2017). Climate response to the Samalas volcanic eruption in 1257 revealed by proxy records. *Nature Geoscience*, *10*(2), 123–128. https://doi.org/10.1038/ngeo2875

Guo, S., Bluth, G. J. S., Rose, W. I., Watson, I. M., & Prata, A. J. (2004). Re-evaluation of SO_2 release of the 15 June 1991 Pinatubo eruption using ultraviolet and infrared satellite sensors. *Geochemistry, Geophysics, Geosystems*, *5*(4), Q04001. https://doi.org/10.1029/2003GC000654

Larsen, J. F., Neal, C., Schaefer, J., Beget, J., & Nye, C. (2007). Late pleistocene and holocene caldera-forming eruptions of Okmok Caldera, Aleutian Islands, Alaska. In *Volcanism and subduction: The Kamchatka region* (pp. 343–364). American Geophysical Union (AGU). https://doi.org/10.1029/172GM24

Luterbacher, J., Werner, J. P., Smerdon, J. E., Fernández-Donado, L., González-Rouco, F. J., Barriopedro, D., et al. (2016). European summer temperatures since Roman times. *Environmental Research Letters*, *11*(2), 024001. https://doi.org/10.1088/1748-9326/11/2/024001

Marshall, L. R., Schmidt, A., Johnson, J. S., Mann, G. W., Lee, L. A., Rigby, R., & Carslaw, K. S. (2021). Unknown eruption source parameters cause large uncertainty in historical volcanic radiative forcing reconstructions. *Journal of Geophysical Research: Atmospheres*, *126*(13), e2020JD033578. https://doi.org/10.1029/2020JD033578

McConnell, J. R., Sigl, M., Plunkett, G., Burke, A., Kim, W. M., Raible, C. C., et al. (2020). Extreme climate after massive eruption of Alaska's Okmok volcano in 43 BCE and effects on the late Roman Republic and Ptolemaic Kingdom. *Proceedings of the National Academy of Sciences*, *117*(27), 15443–15449. https://doi.org/10.1073/pnas.2002722117

Orbe, C., Rind, D., Jonas, J., Nazarenko, L., Faluvegi, G., Murray, L. T., et al. (2020). GISS model E2.2: A climate model optimized for the middle Atmosphere—2. Validation of large-scale transport and evaluation of climate response. *Journal of Geophysical Research: Atmospheres*, *125*(24), e2020JD033151. https://doi.org/10.1029/2020JD033151

Pauling, A. G., Bitz, C. M., & Armour, K. C. (2023). The climate response to the Mt. Pinatubo eruption does not constrain climate sensitivity. *Geophysical Research Letters*, *50*(7), e2023GL102946. https://doi.org/10.1029/2023GL102946

Pearson, C., Sigl, M., Burke, A., Davies, S., Kurbatov, A., Severi, M., et al. (2022). Geochemical ice-core constraints on the timing and climatic impact of Aniakchak II (1628 BCE) and Thera (Minoan) volcanic eruptions. *PNAS Nexus*, *1*(2), pgac048. https://doi.org/10.1093/pnasnexus/pgac048

Rind, D., Orbe, C., Jonas, J., Nazarenko, L., Zhou, T., Kelley, M., et al. (2020). GISS model E2.2: A climate model optimized for the middle Atmosphere—Model structure, climatology, variability, and climate sensitivity. *Journal of Geophysical Research: Atmospheres*, *125*(10), e2019JD032204. https://doi.org/10.1029/2019JD032204

Robock, A. (2000). Volcanic eruptions and climate. *Reviews of Geophysics*, *38*(2), 191–219. https://doi.org/10.1029/1998RG000054

Rowell, C. R., Jellinek, A. M., Hajimirza, S., & Aubry, T. J. (2022). External surface water influence on explosive eruption dynamics, with implications for stratospheric sulfur delivery and volcano-climate feedback. *Frontiers in Earth Science*, *10*, Q04001. https://doi.org/10.3389/feart.2022.788294

Ryan, W. B. F., Carbotte, S. M., Coplan, J. O., O'Hara, S., Melkonian, A., Arko, R., et al. (2009). Global multi-resolution topography synthesis. *Geochemistry, Geophysics, Geosystems*, *10*(3), Q03014. https://doi.org/10.1029/2008GC002332

Schmidt, A., Ostro, B., Carslaw, K. S., Wilson, M., Thordarson, T., Mann, G. W., & Simmons, A. J. (2011). Excess mortality in Europe following a future Laki-style Icelandic eruption. *Proceedings of the National Academy of Sciences of the United States of America*, *108*(38), 15710–15715. https://doi.org/10.1073/pnas.1108569108

Sigl, M., Winstrup, M., McConnell, J. R., Welten, K. C., Plunkett, G., Ludlow, F., et al. (2015). Timing and climate forcing of volcanic eruptions for the past 2,500 years. *Nature*, *523*(7562), 543–549. https://doi.org/10.1038/nature14565

Su, Y., Huber, C., Bachmann, O., Zajacz, Z., Wright, H., & Vazquez, J. (2016). The role of crystallization-driven exsolution on the sulfur mass balance in volcanic arc magmas. *Journal of Geophysical Research: Solid Earth*, *121*(8), 5624–5640. https://doi.org/10.1002/2016JB013184

Tan, M., Liu, T., Hou, J., Qin, X., Zhang, H., & Li, T. (2003). Cyclic rapid warming on centennial-scale revealed by a 2650-year stalagmite record of warm season temperature. *Geophysical Research Letters*, *30*(12), 1617. https://doi.org/10.1029/2003GL017352

Thordarson, T., & Self, S. (2003). Atmospheric and environmental effects of the 1783–1784 Laki eruption: A review and reassessment. *Journal of Geophysical Research*, *108*(D1), AAC7-1–AAC7-29. https://doi.org/10.1029/2001JD002042

Thordarson, T., Self, S., Óskarsson, N., & Hulsebosch, T. (1996). Sulfur, chlorine, and fluorine degassing and atmospheric loading by the 1783–1784 AD Laki (Skaftár Fires) eruption in Iceland. *Bulletin of Volcanology*, *58*(2), 205–225. https://doi.org/10.1007/s004450050136

Toohey, M., & Sigl, M. (2017). Volcanic stratospheric sulfur injections and aerosol optical depth from 500 BCE to 1900 CE. *Earth System Science Data*, *9*(2), 809–831. https://doi.org/10.5194/essd-9-809-2017

Toohey, M., Stevens, B., Schmidt, H., & Timmreck, C. (2016). Easy Volcanic Aerosol (EVA v1.0): An idealized forcing generator for climate simulations. *Geoscientific Model Development*, *9*(11), 4049–4070. https://doi.org/10.5194/gmd-9-4049-2016

Wolfe, B. A. (2001). *Paleohydrology of a catastrophic flood release from Okmok caldera and post-flood eruption history at Okmok Volcano*, Umnak Island. [Thesis]. Retrieved from https://scholarworks.alaska.edu/handle/11122/6716

Zambri, B., Robock, A., Mills, M. J., & Schmidt, A. (2019). Modeling the 1783–1784 Laki eruption in Iceland: 2. Climate impacts. *Journal of Geophysical Research: Atmospheres*, *124*(13), 6770–6790. https://doi.org/10.1029/2018JD029554

Zimmer, M. M., Plank, T., Hauri, E. H., Yogodzinski, G. M., Stelling, P., Larsen, J., et al. (2010). The role of water in generating the calc-alkaline trend: New volatile data for Aleutian magmas and a New Tholeiitic Index. *Journal of Petrology*, *51*(12), 2411–2444. https://doi.org/10.1093/petrology/egq062

References From the Supporting Information

Cadoux, A., Scaillet, B., Bekki, S., Oppenheimer, C., & Druitt, T. H. (2015). Stratospheric Ozone destruction by the Bronze-Age Minoan eruption (Santorini volcano, Greece). *Scientific Reports*, *5*(1), 12243. https://doi.org/10.1038/srep12243

Costa, F., Scaillet, B., & Gourgaud, A. (2003). Massive atmospheric sulfur loading of the AD 1600 Huaynaputina eruption and implications for petrologic sulfur estimates. *Geophysical Research Letters*, *30*(2), 1068. https://doi.org/10.1029/2002GL016402

Dietterich, H., & de Silva, S. (2010). Sulfur yield of the 1600 eruption of Huaynaputina, Peru: Contributions from magmatic, fluid-phase, and hydrothermal sulfur. *Journal of Volcanology and Geothermal Research*, *197*(1), 303–312. https://doi.org/10.1016/j.jvolgeores.2010.01.003

Dull, R. A., Southon, J. R., Kutterolf, S., Anchukaitis, K. J., Freundt, A., Wahl, D. B., et al. (2019). Radiocarbon and geologic evidence reveal Ilopango volcano as source of the colossal 'mystery' eruption of 539/40 CE. *Quaternary Science Reviews*, *222*, 105855. https://doi.org/10.1016/j.quascirev.2019.07.037

Finney, B., Turner, S., Hawkesworth, C., Larsen, J., Nye, C., George, R., et al. (2008). Magmatic differentiation at an Island-arc caldera: Okmok volcano, Aleutian Islands, Alaska. *Journal of Petrology*, *49*(5), 857–884. https://doi.org/10.1093/petrology/egn008

Gerlach, T. M., Westrich, H. R., Symonds, R. B., Newhall, C. G., & Punongbayan, R. S. (1996). Pre–eruption vapor in magma of the climactic Mount Pinatubo eruption: Source of the giant stratospheric sulfur dioxide cloud. In *Fire and mud. Eruptions and lahars of mount Pinatubo, Philippines* (pp. 415–434). University of Washington Press.

Gertisser, R., Self, S., Thomas, L. E., Handley, H. K., Van Calsteren, P., & Wolff, J. A. (2012). Processes and timescales of magma genesis and differentiation leading to the great Tambora eruption in 1815. *Journal of Petrology*, *53*(2), 271–297. https://doi.org/10.1093/petrology/egr062

Hauri, E., Wang, J., Dixon, J. E., King, P. L., Mandeville, C., & Newman, S. (2002). SIMS analysis of volatiles in silicate glasses: 1. Calibration, matrix effects and comparisons with FTIR. *Chemical Geology*, *183*(1), 99–114. https://doi.org/10.1016/S0009-2541(01)00375-8

Iacovino, K., Ju-Song, K., Sisson, T., Lowenstern, J., Kuk-Hun, R., Jong-Nam, J., et al. (2016). Quantifying gas emissions from the "millennium eruption" of Paektu volcano, democratic people's Republic of Korea/China. *Science Advances*, *2*(11), e1600913. https://doi.org/10.1126/sciadv.1600913

Lloyd, A. S., Plank, T., Ruprecht, P., Hauri, E. H., & Rose, W. (2013). Volatile loss from melt inclusions in pyroclasts of differing sizes. *Contributions to Mineralogy and Petrology*, *165*(1), 129–153. https://doi.org/10.1007/s00410-012-0800-2

Mandeville, C. W., Carey, S., & Sigurdsson, H. (1996). Magma mixing, fractional crystallization and volatile degassing during the 1883 eruption of Krakatau volcano, Indonesia. *Journal of Volcanology and Geothermal Research*, *74*(3), 243–274. https://doi.org/10.1016/S0377-0273(96)00060-1

Peccia, A., Moussallam, Y., & Plank, T. (2023). Melt inclusion and matrix glass data from the 43 BCE eruption of Okmok Volcano (Version 1.0). *Interdisciplinary Earth Data Alliance (IEDA)*. https://doi.org/10.26022/IEDA/112955

Pouget, M., Moussallam, Y., Rose-Koga, E., & Sigurdsson, H. (2023). A reassessment of the sulfur, chlorine and fluorine atmospheric loading during the 1815 Tambora eruption. *Bulletin of Volcanology*. https://doi.org/10.1007/s00445-023-01683-8

Scaillet, B., Clemente, B., Evans, B. W., & Pichavant, M. (1998). Redox control of sulfur degassing in silicic magmas. *Journal of Geophysical Research*, *103*(B10), 23937–23949. https://doi.org/10.1029/98JB02301

Self, S., Gertisser, R., Thordarson, T., Rampino, M. R., & Wolff, J. A. (2004). Magma volume, volatile emissions, and stratospheric aerosols from the 1815 eruption of Tambora. *Geophysical Research Letters*, *31*(20), L20608. https://doi.org/10.1029/2004GL020925

Smith, V. C., Costa, A., Aguirre-Díaz, G., Pedrazzi, D., Scifo, A., Plunkett, G., et al. (2020). The magnitude and impact of the 431 CE Tierra Blanca Joven eruption of Ilopango, El Salvador. *Proceedings of the National Academy of Sciences of the United States of America*, *117*(42), 26061–26068. https://doi.org/10.1073/pnas.2003008117

Thordarson, T., Miller, D. J., Larsen, G., Self, S., & Sigurdsson, H. (2001). New estimates of sulfur degassing and atmospheric mass-loading by the 934 AD Eldgjá eruption, Iceland. *Journal of Volcanology and Geothermal Research*, *108*(1), 33–54. https://doi.org/10.1016/S0377-0273(00)00277-8

Toplis, M. J. (2005). The thermodynamics of iron and magnesium partitioning between olivine and liquid: Criteria for assessing and predicting equilibrium in natural and experimental systems. *Contributions to Mineralogy and Petrology*, *149*(1), 22–39. https://doi.org/10.1007/s00410-004-0629-4

Vidal, C. M., Métrich, N., Komorowski, J.-C., Pratomo, I., Michel, A., Kartadinata, N., et al. (2016). The 1257 Samalas eruption (Lombok, Indonesia): The single greatest stratospheric gas release of the Common Era. *Scientific Reports*, *6*(1), 34868. https://doi.org/10.1038/srep34868

Waters, L. E., & Lange, R. A. (2015). An updated calibration of the plagioclase-liquid hygrometer-thermometer applicable to basalts through rhyolites. *American Mineralogist*, *100*(10), 2172–2184. https://doi.org/10.2138/am-2015-5232

Witter, J. B., & Self, S. (2007). The Kuwae (Vanuatu) eruption of AD 1452: Potential magnitude and volatile release. *Bulletin of Volcanology*, *69*(3), 301–318. https://doi.org/10.1007/s00445-006-0075-4